Microstrip Discontinuity Capacitances for Right-Angle Bends, T Junctions, and Crossings

PETER SILVESTER AND PETER BENEDEK

Abstract—**The integral equations governing the electrostatics of the excess charge distribution near microstrip right-angle bends, T junctions, and crossings are formulated and subsequently solved by a projective method. Extensive discontinuity capacitances are presented in graphical form. Where possible, the data are compared to the available experimental results.**

Introduction

NUMEROUS papers have been published, mostly during the past year, treating various microstrip discontinuities such as open circuits [1]–[7], gaps [1], [8]–[10], and steps [9]–[12]. In earlier papers by the authors, a new method capable of determining the microstrip discontinuity capacitances for open circuits [7], gaps, and steps [10] has been presented. This method determines the excess discontinuity capacitance directly, so that the overall accuracy realized does not suffer degradation from subtraction of nearly equal numbers. This approach can be readily extended to other structures, such as microstrip right-angle bends, T junctions, and crossings, for which the available data are very scarce.

Definitions and Methodology

The best way to introduce the methodology utilized is by actually obtaining the governing integral equations for the excess charges, and hence excess capacitances, at various discontinuities. First, symbols are defined and a key artifice is described. Let $\phi_\infty^{(1)}(P_x)$ denote the potential, at a point P_x in the plane of the microstrip resulting from an infinite microstrip-like charge distribution $\sigma_\infty^{(1)}(P_x')$, i.e., a charge distribution of exactly the form that results when an infinitely long microstrip line is electrostatically charged. The subscript x on the charge and potential coordinates P_x' and P_x indicates that the axis of the microstrip is parallel to the x axis, while the superscript 1 indicates a microstrip of width-to-height ratio $(w/h)_1$. When the meaning is obvious both of these will be omitted. Therefore

$$\phi_\infty^{(1)}(P_x) = \int \sigma_\infty^{(1)}(P_x')G_\infty(P_x; P_x')\,dP_x'. \tag{1}$$

$G_\infty(P_x; P_x')\,dP_x'$ is the Green's function appropriate to the dielectric substrate employed (see (3) following).

Now let $\phi_\xi^{(1)}(P_x)$ represent the potential, in the plane of the microstrip, associated with a microstrip-like charge-density distribution with a sudden polarity reversal in the charge at $x=\xi$. It can be shown that

$$\phi_\xi^{(1)}(P_x) = \int \sigma_\infty^{(1)}(P_x')G_\xi(P_x; P_x')\,dP_x'. \tag{2}$$

Manuscript received August 8, 1972; revised December 15, 1972.

The authors are with the Department of Electrical Engineering, McGill University, Montreal, Quebec, Canada.

The Green's function required in (1) is given by

$$G_\infty(y, y') = \frac{1}{2\pi(\epsilon_0+\epsilon_1)}\sum_{n=1}^{\infty} K^{n-1}\log\frac{4n^2+\left(\frac{y-y'}{h}\right)^2}{4(n-1)^2+\left(\frac{y-y'}{h}\right)^2} \tag{3}$$

where y, y' are potential and charge coordinates in the cross-sectional plane of the microstrip parallel to the microstrip, while that required in (2) is

$$G_\xi(x, y; y') = \frac{1-K}{4\pi\epsilon_0}\left[f(0) - (1-K)\sum_{n=1}^{\infty} K^{n-1}f(n)\right] \tag{4}$$

where

$$f(n) = \log\frac{\sqrt{(x-\xi)^2+(y-y')^2+4n^2h^2}+(x-\xi)}{\sqrt{(x-\xi)^2+(y-y')^2+4n^2h^2}-(x-\xi)}. \tag{5}$$

The Green's function $G_\xi(x, y; y')$ represents the potential value at any point (x, y) of the top of the substrate, when a unit line charge with sudden polarity reversal at $x=\xi$ is placed at y'.

The charge distribution that causes $\phi_\xi^{(1)}$ is exactly the same as $\sigma_\infty^{(1)}(P_x')$ over the interval (ξ, ∞) and equal to $-\sigma_\infty^{(1)}(P_x')$ over the interval $(-\infty, \xi)$. While this situation may be physically difficult to realize, there is no mathematical objection to it. This simple artifice holds the key to the useful formulation of the excess charge problem, as will be shown in the following.

To evaluate the integral in (2), note that the charge distribution resulting from (1) is of the form given by

$$\sigma_\infty(y') = \frac{1}{\sqrt{1-y'^2}}\sum_{i=1}^{k} a_i f_i(y') \tag{6}$$

where

$$f_j(y') = \prod_{i=1}^{j-1}\left[\left(\frac{i}{j-1}\right) - y'^2\right], \qquad j > 1$$
$$1, \qquad j = 1. \tag{7}$$

Note that the Green's function in (4) has a singularity at $y=y'$, while the ratio

$$r_\xi(y; y') = \frac{G_\xi(x, y; y')}{\log\frac{|y-y'|}{|y-y'|+1}} \tag{8}$$

is no longer singular. Substituting into the integration to be

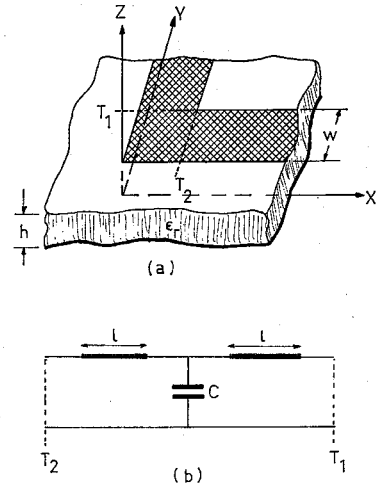

Fig. 1. Microstrip right-angle bend together with equivalent circuit proposed by Stephenson and Easter [13].

performed in (2)

$$\phi_\xi^{(1)}(x, y) = \sum_{i=1}^{k} a_i \int_{-1}^{1} \frac{\log \dfrac{|y-y'|}{|y-y'|+1}}{\sqrt{1-y'^2}} f_i(y') r_\xi(y; y')\, dy'. \quad (9)$$

In this integrand $f_i(y')r_\xi(y; y')$ is nonsingular over the interval $y' \in [-1, 1]$; all the singularities are incorporated in the weight function $\log [|y-y'|/(|y-y'|+1)]/\sqrt{1-y'^2}$. Gaussian quadrature formulas with this weight can be developed for each y. This work is confined to microstrips assumed to be of zero thickness.

Microstrip Right-Angle Bends

For the case of a microstrip right-angle bend, the only data available appear to be the experimental results of Stephenson and Easter [13]. Their equivalent circuit includes a shunt capacitance to account for charge accumulation at the corner, and series lengths of transmission lines on either side to account for the increase in current path length around the corner. This circuit, together with the reference planes used, is shown in Fig. 1. Stephenson and Easter devised two types of resonant measurements: 1) two 90° corners incorporated into a closed-ring resonator; 2) a right-angle bend in a symmetrical open-ended resonator. At various frequencies, voltage maxima or minima occur at the corners, and the two unknowns in the model can be evaluated.

The excess charges which constitute C_{bend} are due to the potential residual, when two microstrip-type charge distributions that exist on the arms of a right-angle bend up to terminal planes T_1 and T_2, as shown in Fig. 1.

Let $\frac{1}{2}\phi_\infty(P_x)$ be the potential corresponding to an infinite microstrip-like charge distribution of $\frac{1}{2}\sigma_\infty(P_x')$ parallel to the x axis. Also let $\frac{1}{2}\phi_{1.0}(P_x)$ represent the potential corresponding to a microstrip-like charge distribution with a polarity reversal at $x=1.0$. Therefore, the potential corresponding to a microstrip-like charge on the interval $x \in (1, \infty)$ is, by superposition, $\frac{1}{2}[\phi_\infty(P_x)+\phi_{10}.(P_x)]$. Similarly, in the y direction, the potential corresponding to a microstrip-like charge on the interval $y \in (1, \infty)$ is $\frac{1}{2}[\phi_\infty(P_y)+\phi_{1.0}(P_y)]$. By superposition one can generate microstrip-like distributions parallel to the positive x and y axes up to terminal planes T_1 and T_2. Therefore, the potential residual required is

$$\phi_x^{\text{bend}}(P) = \phi_\infty - \tfrac{1}{2}[\phi_\infty(P_x) + \phi_{1.0}(P_x) + \phi_\infty(P_y) + \phi_{1.0}(P_y)] \quad (10)$$

while the governing integral equation for the excess charge is

$$\phi_x^{\text{bend}}(P) = \int \sigma_x^{\text{bend}}(P') G^{\text{bend}}(P; P')\, dP'. \quad (11)$$

Although the indicated integration is over the entire bend including the semi-infinite arms, both potential residual and excess charge fall to zero on moving away from the discontinuity region.

The Green's function can be shown, in a manner analogous to that used for the rectangular plates separated by a dielectric sheet [14], to be

$$G^{\text{bend}}(x, y; x', y') = \frac{1}{2\pi(\epsilon_0+\epsilon_1)}\left[f(0) - (1-K)\sum_{n=1}^{\infty} K^{n-1} f(n)\right] \quad (12)$$

where

$$f^{\text{bend}}(n) = \left[(2n)^2 + \left(\frac{x-x'}{h}\right)^2 + \left(\frac{y-y'}{h}\right)^2\right]^{-1/2} \quad (13)$$

and the bend capacitance is calculated from

$$C_{\text{bend}} = \int \sigma_x^{\text{bend}}(P')\, dP'. \quad (14)$$

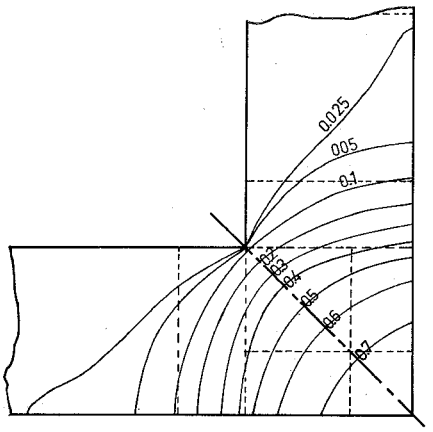

Fig. 2. Potential residual near a microstrip right-angle bend ($w_1/h=1.0$ and $\epsilon_r=1.0$).

A typical residual voltage for dielectric substrate of $\epsilon_r=1.0$ and microstrip width-to-height ratio $w/h=1$ is shown in Fig. 2. Not shown in this figure is that by moving further away from the discontinuity, some small amount of negative potential residual appears and then it dies down to zero. This is due to the interaction between the two normal microstrip-like distributions and is most noticeable for small ϵ_r and w/h. Numerical experiments indicate that the most significant part of the excess charge is located near the outer edge of the corner region. Thus, the typical discretization used is also shown in Fig. 2. Although the symmetry about the 45° angle is not accounted for in (13), the discretization of the region is done so

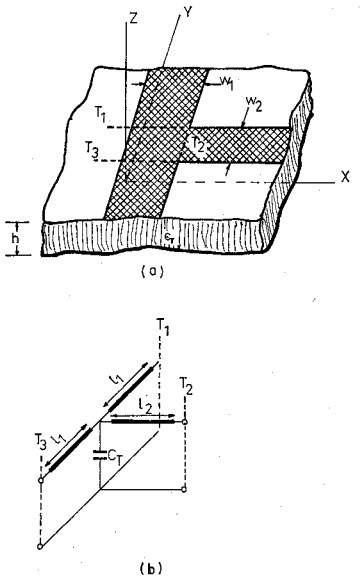

Fig. 3. Microstrip T junction together with its equivalent circuit.

that full advantage may be taken of this symmetry during computation.

Microstrip T Junctions

In the case of microstrip T junctions, five sources of data were located. Stinehelfer [1] and Troughton [2] presented experimental results. They both performed transmission loss measurements on microstrip T structures to determine the electrical length of a stub; comparing this with the physical length, the "electrical defining plane" [2] for the stub can be determined. Stinehelfer presented results obtained using quarter-wavelength-long short-circuited stubs, while Troughton used quarter- and three-quarter-wavelength-long open-circuited stubs. Both investigators indicated that a correction to the separation between two stubs is also required.

On the theoretical side, Leighton and Milnes [15], as well as Wolff, Kompa, and Mehran [11], [12], used a parallel-plate waveguide approximation valid over a restricted range of parameters, with magnetic walls on the sides. Leighton and Milnes then used a Babinet equivalent of this model to obtain a new model with a T junction equivalent circuit previously determined by Marcuvitz [16]. Wolff, Kompa, and Mehran, on the other hand, matched wave components at the discontinuity planes and were able to obtain scattering coefficients for the T junction.

The simplest equivalent circuit for the T junction is an outcropping of the work of experimentalists. The microstrip T junction, together with this model, is shown in Fig. 3. The lengths of transmission lines are used to correct for the electrical defining planes of the stub and main lines, while the shunt capacitor accounts for the charge surplus or deficiency at the junction.

The potential residual, causing a charge surplus or deficiency at the T junction, is that due to three microstrip-like charge distributions on the arms of the T structure, up to the terminal planes T_1, T_2, and T_3, shown in Fig. 3(a). To evaluate this potential residual, take a microstrip-like charge distribution $\frac{1}{2}\sigma_\infty^{(2)}(P_x')$, of width-to-height ratio (w_2/h), parallel to the x axis, with corresponding potential $\frac{1}{2}\phi_\infty^{(2)}(P_x)$, given by (1). Take another microstrip-like charge distribution $\frac{1}{2}\sigma_\infty^{(2)}(P_x')$, having a polarity reversal at $x=w_1$, with the corresponding potential $\frac{1}{2}\phi_{w_1}^{(2)}(P_x)$, given by (2). The superposition of these two distributions yields a microstrip-like charge of width-to-height ratio (w_2/h) on the interval $x\in[w_1, \infty]$ and a corresponding potential of $\frac{1}{2}[\phi_\infty^{(2)}(P_x)+\phi_{w_1}^{(2)}(P_x)]$. Similarly, in the y direction, an infinite microstrip-like charge distribution $\sigma_\infty^{(1)}(P_x')$ together with charge distributions $\frac{1}{2}\sigma_\infty^{(1)}(P_y')$ with polarity reversals at $y=1.0$ and -1.0 are required. The respective potentials, by (1) and (2), are $\phi_\infty^{(1)}(P_y)$, $\frac{1}{2}\phi_{1.0}^{(1)}(P_y)$, and $\frac{1}{2}\phi_{-1.0}^{(1)}(P_y)$. The superposition of these three yields a microstrip-like distribution on the two intervals $|y|>1.0$, with corresponding potential $\{\phi_\infty^{(1)}(P_y)+\frac{1}{2}[\phi_{1.0}^{(1)}(P_y)-\phi_{-1.0}^{(1)}(P_y)]\}$.

Now, superposing the two resulting distributions, microstrip-like charges are generated on the arms of the T structure up to the terminal planes T_1, T_2, and T_3. Therefore, the potential residual, in this case, is

$$\phi_x^T(P) = \phi_\infty - \left\{\tfrac{1}{2}[\phi_\infty^{(2)}(P_x) + \phi_{w_1}^{(2)}(P_x)] + \phi_\infty^{(1)}(P_y) + \tfrac{1}{2}[\phi_{1.0}^{(1)}(P_y) - \phi_{-1.0}^{(1)}(P_y)]\right\} \quad (15)$$

while the integral equation governing the excess charge is

$$\phi_x^T(P) = \int \sigma_x^T(P')G^T(P; P')\, dP'. \quad (16)$$

In (16) both the potential residual and the excess charge fall to zero moving away from the discontinuity, so that integration over finite regions suffices.

The Green's function $G^T(P; P')$ is the same as $G^{\text{bend}}(P; P')$ given by (12); however

$$f^T(n) = \left[(2n)^2 + \left(\frac{x-x'}{h}\right)^2 + \left(\frac{y-y'}{h}\right)^2\right]^{-1/2} + \left[(2n)^2 + \left(\frac{x-x'}{h}\right)^2 + \left(\frac{y+y'}{h}\right)^2\right]^{-1/2} \quad (17)$$

and the T junction capacitance is given by

$$C_T = \int \sigma_x^T(P')\, dP'. \quad (18)$$

The potential residual on a dielectric substrate of $\epsilon_r=9.9$, with main line $(w_1/h)=1.0$ and stub line $(w_2/h)=1.0$ is shown in Fig. 4. In this case regions of negative residuals are much more pronounced than for the right-angle bend. A typical discretization of the region is also shown in Fig. 4.

Microstrip Crossings

For microstrip crossings, it appears that the only published source of data is that obtained experimentally by Stinehelfer [1]. He performed transmission loss measurements, as in the case of T junctions, on a pair of quarter-wavelength short-circuited stubs placed back to back, so as to determine the electrical lengths of the stubs. Similarly, a correction to the physical distance between a pair of crossings was noted.

The circuit model shown in Fig. 5(b) for the crossing shown in Fig. 5(a) was arrived at as a consequence of the results obtained in the above experiments The lengths of transmission lines correct for the electrical lengths of the stubs and their electrical spacing from various other discontinuities. The shunt capacitor C_+ takes care of the charge surplus or deficiency near the crossing.

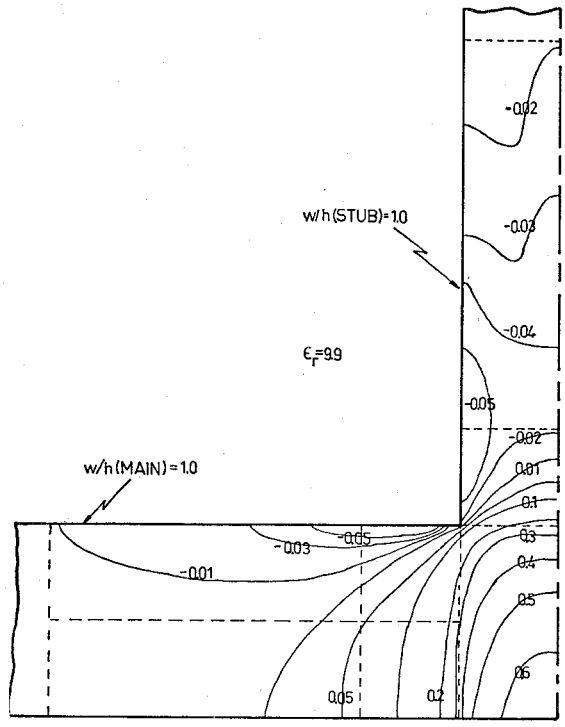

Fig. 4. Potential residual near a microstrip T junction ($w_1/h=1.0$, $w_2/h=1.0$, and $\epsilon_r=9.9$).

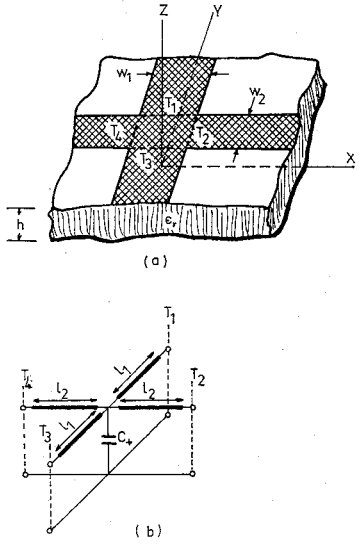

Fig. 5. Microstrip crossing together with its equivalent circuit.

As in earlier discontinuities, the potential residual sought is obtained from the potential due to microstrip-like charge distributions of the four arms of the crossing, up to the reference planes T_1, T_2, T_3, and T_4.

To obtain such a distribution, an infinite microstrip-like charge $\sigma_\infty^{(2)}(P_x')$ of width-to-height ratio (w_2/h) is required. Also needed are two charge distributions $\frac{1}{2}\sigma_\infty^{(2)}(P_x')$ with polarity reversals at $x=w_1/2$ and $-w_1/2$. The corresponding potential distributions, given by (1) and (2) are $\phi_\infty^{(2)}(P_x)$, $\phi_{w_1/2}^{(2)}(P_x)$, and $\phi_{-w_1/2}^{(2)}(P_x)$, respectively. By superposition, microstrip-like charge densities of (w_2/h) are obtained on the two intervals $|x|>w_1/2$, and the resulting potential is

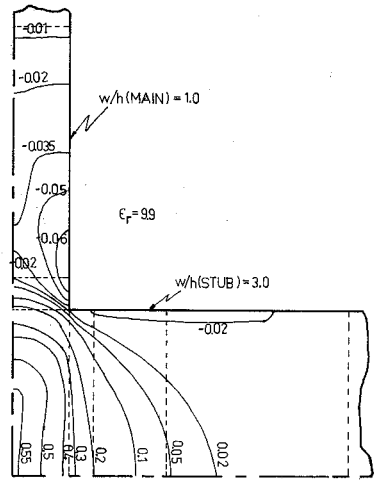

Fig. 6. Potential residual near a microstrip crossing ($w_1/h=3$, $w_2/h=1$, and $\epsilon_r=9.9$).

$\{\phi_\infty^{(2)}(P_x)+\frac{1}{2}[\phi_{w_1/2}^{(2)}(P_x)-\phi_{-w_1/2}^{(2)}(P_x)]\}$. Similarly, the potential corresponding to microstrip-like charge distribution $\sigma_\infty^{(1)}(P_y')$ of width-to-height ratio (w_1/h) on the intervals $|y|>1.0$ is $\{\phi_\infty^{(1)}(P_y)+\frac{1}{2}[\phi_{1.0}^{(1)}(P_y)-\phi_{-1.0}^{(1)}(P_y)]\}$.

By superposition of these two resultant distributions, microstrip-like charge densities of appropriate width-to-height ratios are generated, on the arms of the crossing, up to the four terminal planes. Therefore, the potential residual sought is

$$\phi_x^+(P)=\phi_\infty-\{\phi_\infty^{(1)}(P_y)+\tfrac{1}{2}[\phi_{1.0}^{(1)}(P_y)-\phi_{-1.0}^{(1)}(P_y)]+\phi_\infty^{(2)}(P_x)+\tfrac{1}{2}[\phi_{w_1/2}^{(2)}(P_x)-\phi_{-w_1/2}^{(2)}(P_x)]\} \quad (19)$$

and the integral equation governing the excess charge is

$$\phi_x^+(P)=\int \sigma_x^+(P')G^+(P;P')\,dP'. \quad (20)$$

As in earlier instances, integration over a finite region is sufficient, since both potential residual and charge-density distribution go to zero on moving away from the discontinuity.

The Green's function given by (12) is also valid for $G^+(P;P')$ with

$$f^+(n)=\left[(2n)^2+\left(\frac{x-x'}{h}\right)^2+\left(\frac{y-y'}{h}\right)^2\right]^{-1/2}+\left[(2n)^2+\left(\frac{x-x'}{h}\right)^2+\left(\frac{y+y'}{h}\right)^2\right]^{-1/2}+\left[(2n)^2+\left(\frac{x+x'}{h}\right)^2+\left(\frac{y-y'}{h}\right)^2\right]^{-1/2}+\left[(2n)^2+\left(\frac{x+x'}{h}\right)^2+\left(\frac{y+y'}{h}\right)^2\right]^{-1/2} \quad (21)$$

while the crossing capacitance is given by

$$C_+=\int \sigma_x^+(P')\,dP'. \quad (22)$$

In Fig. 6 the potential residual for a stub of $(w_1/h)=3$ and main line of $(w_2/h)=1$, on a substrate of relative dielectric

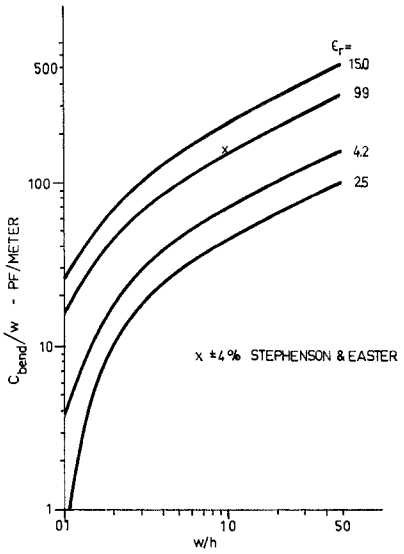

Fig. 7. Microstrip bend capacitances normalized to strip width as a function of width-to-height ratio and substrate permittivity.

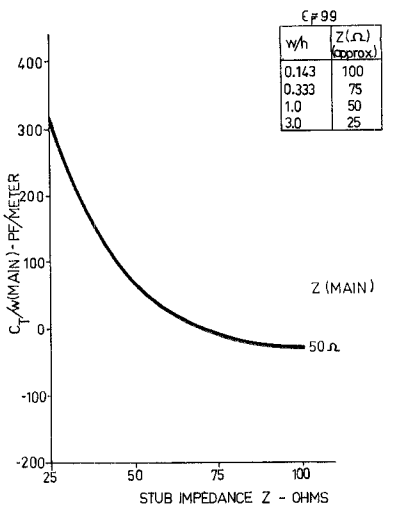

Fig. 8. Microstrip T junction capacitances, normalized to main-line width, as a function of stub-line impedance.

constant $\epsilon_r = 9.9$, is shown. Also shown in the figure is a typical discretization of the region.

Results and Comparison with Existing Data

The bend capacitances obtained by Stephenson and Easter [13] by means of their two resonant measurements agree with each other in order of magnitude only. However, the two types of measurements, both 90° bends and chamfered corners for a 50-Ω microstrip line on alumina substrate, indicate that the lengths of transmission line in the model of Fig. 1 are negligible.

For various sound reasons, Stephenson and Easter conclude that the result obtained via the right-angle bend in a symmetrical open-ended resonator is the better of the two. Error limits are also indicated. Their measurement, at 10 GHz on 0.5-mm Lucalox with a strip width corresponding to approximately 50-Ω characteristic impedance, is shown in Fig. 7 together with their indicated error limits.

Also shown in Fig. 7 are bend capacitances, calculated by this method, normalized with respect to strip width for various commonly used substrates. As expected, the calculated values are lower than those obtained experimentally. Nevertheless, the close agreement between the results is an indication of the accuracy of the method. Typical computation time on an IBM S360/75 is 50 s for $\epsilon_r = 1.0$ and 110 s for $\epsilon_r = 9.9$.

Stinehelfer's [1] measurements, on quarter-wavelength-long short-circuited stubs, indicate that the electrical length of the stubs is shorter than the physical length, while Troughton's measurements, on quarter- and three-quarter-wavelength open-circuited stubs, indicate that the electrical length of the stub is longer than the physical length. Troughton also indicates that "if the stub is $\lambda/4$ and $3\lambda/4$, Δl (the correction to the physical length) is consistent, but differs from the value found from a half-wavelength stub." In addition to the specific problems in each measurement (such as accurate end-effect correction in Troughton's case, difficulty of determining the exact frequency at which total transmission occurs in Stinehelfer's case, and accurate phase velocity in both cases), part of the discrepancy is resolved considering the model given in Fig. 3(b). If L denotes the physical length of the stub, in Troughton's case already corrected for the end effect, then Troughton measured the frequency at which $(l_2+L)=\lambda/4$, while Stinehelfer measured the conditions under which $\cot[2\pi(l_2+L)/\lambda]=\omega C_T Z$. As a matter of fact, in principle, performing measurements on open- and short-circuited quarter-wavelength stubs, it would be possible to determine both l_2 and C_T. This, however, may be frustrated by the difficulties already enumerated.

The theoretical results of Leighton and Milnes [15] on the approximate model of the microstrip line, are valid over a restricted range of parameters. Since both the model and the reference planes used here are totally different, no comparison was made with their data.

The approximate theoretical results of Wolff, Kompa, and Mehran [11], [12] are in terms of magnitudes of scattering coefficients of the T junction. The data given are for polyguide substrate, relative dielectric constant of $\epsilon_r = 2.33$, and they show very pronounced frequency dependence, especially above 5 GHz. This, at first sight, cannot be explained in terms of the capacitor C_T obtained here. A quick calculation, however, will indicate that at 5 GHz for $\epsilon_r = 2.33$ the wavelength is about 40 mm, while the typical dimensions required for the characteristic impedances utilized range from 4.5 to about 10 mm. For such structures the excess charges occupy a significant fraction of the wavelength, so that the electrostatic approximation is not valid. This argument is further substantiated by their note to the effect that the frequency dependence is small for alumina substrate ($\epsilon_r = 9.9$), where realistic impedances are obtained for smaller width-to-height ratios and the commonly available substrate thicknesses are 0.020 and 0.025 in.

Fig. 8 shows the capacitance C_T normalized to main-line width plotted against stub-line impedance. The behavior of C_T, in that it varies from positive to negative depending whether there is charge deficiency or charge surplus, is similar to that observed experimentally by Matthaei, Young, and Jones [17] in stripline. Due to the variation of the sign of the potential residual, generally speaking, the capacitances thus obtained are expected to have somewhat larger errors than, for example, in the open-circuit case, where the potential

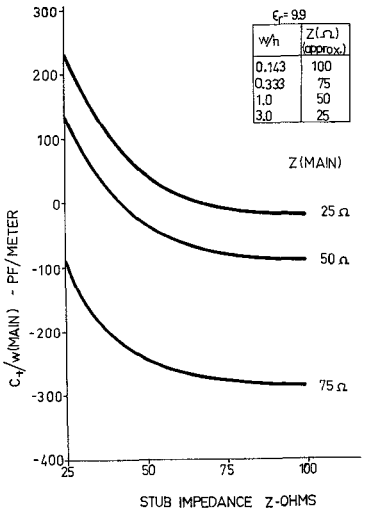

Fig. 9. Microstrip crossing capacitances, normalized to main-line width, as a function of stub-line impedance.

residual is of uniform sign. The central processing unit (CPU) time required on an IBM S360/75 to evaluate C_T on a dielectric substrate of $\epsilon_r = 9.9$ is 3.6 min.

The results given by Stinehelfer [1], done on two short-circuited quarter-wavelength-long stubs back to back, indicate that the electrical length of the stubs is shorter than the physical length. However, arguing as for the T junction, the model given in Fig. 5(b) would indicate that such a measurement in effect determines the frequency at which 2 cot $[2\pi(l_2+L)]/\lambda = \omega C_+ Z$. L is the physical length of the stub. Another transmission loss measurement, on quarter-wavelength-long open-circuited stubs, would give the frequency at which $(l_2+L) = \lambda/4$. In principle, l_2 and C_+ may be determined from two such measurements. The difficulties with such an experimental approach were outlined in [1, sec. 5.7.4]. Using the results given by Stinehelfer, no estimate of C_+ can be made. There appear to be no other data available for comparison.

In the computer program the computational details for the stub and main line are somewhat different. Therefore, interchanging the width-to-height ratios of the stub and main line left C_+ unchanged. This, in a small measure, provided a check on the program details.

Fig. 9 shows crossing capacitance values C_+ normalized to main-line width for various main-line impedances, plotted against stub-line impedance. The stub characteristic impedances range from 25 to 100 Ω. The substrate dielectric constant used is $\epsilon_r = 9.9$. As in the case of T junctions, due to the variation in the sign of the potential residual, generally speaking the errors in capacitance values can be expected to be larger than in those cases where the potential residual is of uniform sign. The computation time required on an IBM S360/75, for C_+ on a relative dielectric constant $\epsilon_r = 9.9$ is about 3.7 min.

Conclusions

Extensive microstrip discontinuity capacitance values are presented. In the case of microstrip right-angle bends the only available experimental result is in close agreement with the calculations. It is hoped that more experimental results will become available in the future.

The methodology utilized can be extended to analyze the electrostatic capacitive effect of virtually any microstrip discontinuity.

References

[1] H. E. Stinehelfer, Sr., "Microstrip circuit design," Tech. Rep. AFAL-TR-69-10, AD 848 947, Feb. 1969.
[2] P. Troughton, "Design of complex microstrip circuits by measurements and computer modeling," *Proc. Inst. Elec. Eng.*, vol. 118, no. 3/4, pp. 469–474, Mar./Apr. 1971.
[3] L. S. Napoli and J. J. Hughes, "Foreshortening of microstrip open circuits on alumina substrates," *IEEE Trans. Microwave Theory Tech.* (Corresp.), vol. MTT-19, pp. 559–561, June 1971.
[4] A. Farrar and A. T. Adams, "Computation of lumped microstrip capacities by matrix methods—Rectangular sections and end effect," *IEEE Trans. Microwave Theory Tech.* (Corresp.), vol. MTT-19, pp. 495–497, May 1971.
[5] ——, "Correction to 'Computation of lumped microstrip capacities by matrix method—Rectangular sections and end effect,'" *IEEE Trans. Microwave Theory Tech.* (Lett.), vol. MTT-20, p. 294, Apr. 1972.
[6] D. S. James and S. H. Tse, "Microstrip end effects," *Electron. Lett.*, pp. 46–47, Jan. 22, 1972.
[7] P. Silvester and P. Benedek, "Equivalent capacitances for microstrip open circuits," *IEEE Trans. Microwave Theory Tech.*, vol. MTT-20, pp. 511–516, Aug. 1972.
[8] M. Maeda, "An analysis of gap in microstrip transmission lines," *IEEE Trans. Microwave Theory Tech.*, vol. MTT-20, pp. 390–396, June 1972.
[9] A. Farrar and A. T. Adams, "Matrix methods for microstrip three-dimensional problems," *IEEE Trans. Microwave Theory Tech.*, vol. MTT-20, pp. 497–504, Aug. 1972.
[10] P. Benedek and P. Silvester, "Equivalent capacitances for microstrip gaps and steps," *IEEE Trans. Microwave Theory Tech.*, vol. MTT-20, pp. 729–733, Nov. 1972.
[11] I. Wolff, G. Kompa, and R. Mehran, "Calculation method for microstrip discontinuities and T-junctions," *Electron. Lett.*, vol. 8, no. 7, pp. 177–179, Apr. 6, 1972.
[12] ——, "Streifenleitungsdiskontinuitaten und-Verzweigungen," *Nachrichtentech. Z.*, vol. 25, no. 5, pp. 217–264, May 1972.
[13] I. M. Stephenson and B. Easter, "Resonant techniques for establishing the equivalent circuits of small discontinuities in microstrip," *Electron. Lett.*, vol. 7, no. 19, pp. 582–584, Sept. 23, 1971.
[14] P. Benedek and P. Silvester, "Capacitance of parallel rectangular plates separated by a dielectric sheet," *IEEE Trans. Microwave Theory Tech.*, vol. MTT-20, pp. 504–510, Aug. 1972.
[15] W. H. Leighton, Jr., and A. G. Milnes, "Junction reactance and dimensional tolerance effects on X-band 3-dB directional couplers," *IEEE Trans. Microwave Theory Tech.*, vol. MTT-19, pp. 818–824, Oct. 1971.
[16] N. Marcuvitz, Ed., *Waveguide Handbook.* New York: Dover, 1965.
[17] G. L. Matthaei, L. Young, and E. M. T. Jones, *Microwave Filters Impedance—Matching Networks and Coupling Structures.* New York: McGraw-Hill, 1964